McLeod, H. O., Jr., and J. M. Campbell, "Natural Gas Hydrates at Pressures to 10000 psia," *Trans. A.I.M.E.*, **222**, 590 (1961).
Musaev, R. M., Candidate's thesis, All-Union Scientific Research Institute for Gas, Moscow, Russia (1966).
Noaker, L. J., and D. L. Katz, "Gas Hydrates of Hydrogen Sulfide-Methane Mixtures," *Trans. A.I.M.E.*, **201**, 237 (1954).
Otto, F. D., and D. B. Robinson, "A Study of Hydrates in the Methane-Propylene-Water System," *AIChE J.*, **6**, 602 (1960).
Parrish, W. R., and J. M. Prausnitz, "Dissociation Pressures of Gas Hydrates Formed by Gas Mixures," *Ind. Eng. Chem. Process. Design Develop.*, **11**, 26 (1972).
Pieroen, A. P., and A. E. Korvezee, "The Lowering of the Three-Phase Equilibrium Temperature in a Binary System Upon the Addition of a Third Component," *Rec. Trav. Chim.*, **81**, 898 (1962).
Robinson, D. B., and B. R. Mehta, "Hydrates in the Propane-Carbon Dioxide-Water System," *J. Can. Petrol. Technol.*, **49**, 642 (1971).
Rouher, O. S., and A. J. Barduhn, "Hydrates of Iso and Normal Butane and Their Mixtures," *Desalination*, **6**, 67 (1969).
Schneider, G. R., and J. Farrar, *O.S.W. Res. Develop. Progr. Rept. No.* 292 (1968).
Unruh, C. H., and D. L. Katz, "Gas Hydrates of Carbon Dioxide-Methane Mixtures," *Petrol. Trans. A.I.M.E.*, **186**, 83 (1949).
Van der Waals, J. H., and J. C. Platteeuw, *Advances in Chemical Physics*, Vol. 2, p. 1, Interscience, New York (1959).
Verma, V. K., J. H. Hand, and D. L. Katz, "Gas Hydrates from Liquid Hydrocarbons (methane-propane-water system)," paper presented at *GVC/AIChE* Joint Meeting, Munich, Germany, (Sept. 17, 1974).
Wilcox, W. I., D. B. Carson, and D. L. Katz, "Natural Gas Hydrates," *Ind. Eng. Chem.*, **33**, 662 (1941).
Wu, B.-J., D. B. Robinson, and H.-J. Ng, "Three and Four Phase Hydrate Forming Conditions in the Methane-Isobutane-Water System," *J. Chem. Therm.*, 8(5), 461 (1976).

Manuscript received January 14, 1976; revision received and accepted March 29, 1976.

The Fluid Mechanics and Heat Transfer of Injection Mold Filling of Thermoplastic Materials

YOUTI KUO

Electrical Components Division
Bendix Corporation
Sidney, New York

MUSA R. KAMAL

Department of Chemical Engineering
McGill University
Montreal, Quebec

For injection flow of thermoplastic material in thin cavities, with some minor restrictions, both pressure and stream function obey Laplace equations. An analytical-numerical method, with a generalized viscous model used, is developed for determining the shape of a progressing flow front and for computing flow quantities and temperature distributions. Specifically, flows in a rectangular cavity are solved and compared to experiments.

SCOPE

The injection molding process is a very important fabricating method in producing plastic articles. Its technique, however, has been essentially an art, and the trial-and-error approach employed in production often cannot cope with variations in resin properties, complexity of molding geometries, and variations in process parameters. To seek optimum control of the molding variables, a model simulation of the process is highly desirable as it may enable the prediction of the filling behavior and mechanical properties of the finished products.

For convenience of analysis. the molding process can be divided into filling, packing, and cooling stages because of their respective characteristics, as outlined by Kamal et al. (1975). This paper deals with the fluid mechanics and heat transfer aspect of the filling stage of thermoplastic materials. Analyses of subsequent stages, which require the temperature and flow fields at the end of filling as given initial conditions, will be reported in separate papers.

Polymer melts are viscoelastic and compressible, and injection flows are three dimensional, unsteady, nonisothermal, and involve a free surface. An analysis involving every factor of the flow and the material is extremely difficult. In view of the fact that molded plastic parts are usually combinations of various thin sections, an analysis dealing with thin cavities is realistic and may lead to simplification of the problem. Such an approach has been employed in many typical numerical analyses, using finite difference techniques by Kamal and Kenig (1972), Wu et al. (1974), Lord and Williams (1975), and other characteristic studies by Richardson (1972) and White (1975) on injection mold filling. Some experimental studies by Menges and Wubken (1973), White and Dee (1974), and Schmidt (1974) used thin cavities.

In this paper, the implications of thin cavities is explored further. Based on thin cavity approximations, an energy equation and equations of stream function and pressure (two dimensional) are developed for solving flow quantities and temperature distributions in complex

cavities. The analysis considers general dependency of viscosity on both shear rate and temperature.

For testing the theory and computations, experimental results obtained by Doan (1974) were used for comparison. Shown in this paper are the results of using commercial polystyrene and polyethylene resins in filling a rectangular cavity .318 cm × 6.35 cm × 22.9 cm in size through a small gate under wide variations of molding conditions.

CONCLUSIONS AND SIGNIFICANCE

With assumptions of both viscosity and temperatures varying strongly across a narrow cavity but weakly in the flow direction, it is shown that both the pressure and the stream functions obey Laplace equations even for thermoplastic flows. Physically the equations apply to cases involving small variations of temperature and flow area in the flow direction. According to potential theory, the streamlines and isopressure lines are orthogonal. This condition, observed also experimentally, enables the determination of flow front shapes theoretically by using well-established techniques such as conformal mapping.

Moreover, the analytical-numerical method developed enables use of a generalized viscous model. Good agreement was obtained between computational results and experimental measurements on pressure distribution and progression of flow front. Findings of particular interest are that profiles of the flow fronts vary more with effective width of the gate but less with the type of resin, and that the temperature gradient in the flow direction is small. The latter finding is consistent with our prior assumption regarding the temperature field for the development of working equations.

ANALYSIS

Thin Cavity Approximations

The implications of thin cavity approach are:

1. The ratio of thickness to width is much less than unity.
2. The variation of pressure and the transverse velocity near the flow front across the narrow gap are negligible.
3. The gradients of (extra) stresses are much larger in the thickness direction than in flow directions.
4. The gradients of viscosity, temperature, and velocity vary strongly across the thin gap but vary weakly in flow directions.
5. Inertia force is negligible when compared to a very large viscous force; that is, the Reynolds number is much less than unity.
6. Surface tension and normal stress effects on the profiles of a free surface (on the x, y plane, see Figure 1) are insignificant owing to the small change of curvature.

The above approximations are direct consequences of a thin cavity approach. Most significantly, the injection flow is thus simplified as two dimensional. In this case, a Newtonian velocity solution is the solution to a viscoelastic fluid of second order (Tanner, 1966). It is expected that a purely non-Newtonian viscous solution can be the first-order solution to a constitutive equation for a nearly viscometric flow (Kuo, 1973). Furthermore, it is assumed that the stress relaxation, which is important in viscoelastic flows involving sharp change of stresses, does not play a significant role here since the polymer melt undergoes strong shearing continuously when pushed from a gate into the narrow cavity. In the present approach, the effect of the elongational rate on the viscosity in the radial flow region (Laurencena and Williams, 1974) is also ignored owing to dominant roles of the shear rate and the shear stress gradient mentioned previously. Its effect may diminish if the thin cavity approximation is confined to a distance away from the flow source or the gate. For simplicity, the analysis to follow will treat the melt as incompressible during the filling stage. The above approximations imply that an analysis with a generalized viscous model used may yield satisfactory solutions to the injection flows of thermoplastics in thin cavities.

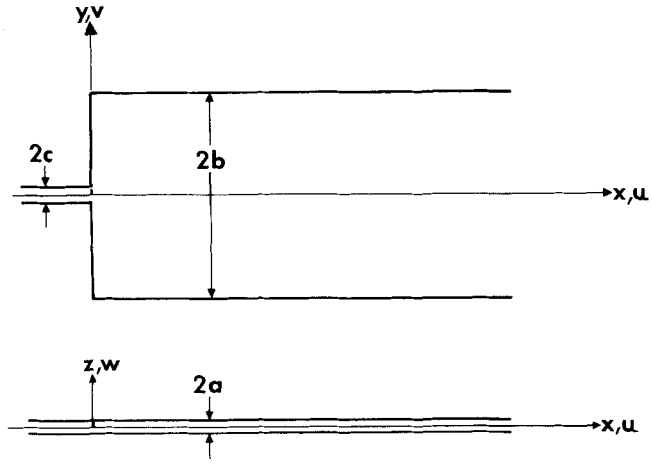

Fig. 1. Sketch of the rectangular cavity and the coordinate system.

Governing Equations

In the subsequent derivations, the following type of constitutive equation for the shear stress τ will be used:

$$\tau = \dot{\gamma}\eta(T, \dot{\gamma}^2) \tag{1}$$

in which η is a general viscosity function depending on both the temperature T and the shear rate $\dot{\gamma}$. The scalar value of the shear rate is defined as

$$\dot{\gamma}^2 = \left(\frac{\partial u}{\partial z}\right)^2 + \left(\frac{\partial v}{\partial z}\right)^2 \tag{2}$$

where the velocity components u and v are in accordance with the Cartesian coordinate system x, y, z as shown in Figure 1. Note that the coordinate z is in the thickness direction of the cavity.

As a result of thin cavity approximations outlined previously, the momentum equations can be simplified to

$$-\frac{\partial P}{\partial x} + \frac{\partial}{\partial z}\left(\eta \frac{\partial u}{\partial z}\right) = 0(\sigma^2) \tag{3}$$

$$-\frac{\partial P}{\partial y} + \frac{\partial}{\partial z}\left(\eta \frac{\partial v}{\partial z}\right) = 0(\sigma^2) \tag{4}$$

The terms inside the parentheses on the left-hand sides are the x, y components of the shear stress. The above two equations show the balance of the pressure and the shear gradients. The roles of gradients of normal stresses and the inertia force diminish as the thickness/width ratio σ becomes very small. It can be shown that the ignored terms are of second order as indicated above.

To solve for the velocity components, an integration of Equations (3) and (4) with respect to z with a no-slip boundary condition on the walls $z = \pm a$ yields

$$u = \frac{\partial P}{\partial x}\Phi \tag{5}$$

$$v = \frac{\partial P}{\partial y}\Phi \tag{6}$$

where

$$\Phi = \int_\alpha^z \frac{z'}{\eta(x, y, z', t)}\,dz' \tag{7}$$

Note that the derived function Φ may vary strongly in z but weakly in x and y directions as the viscosity η does.

In order to carry out the integration, the viscosity profile must be obtained. With some manipulation of Equations (3) and (4), we obtain

$$\eta(T, \dot\gamma^2)\dot\gamma^2 = \left[\left(\frac{\partial P}{\partial x}\right)^2 + \left(\frac{\partial P}{\partial y}\right)^2\right] z^2 \tag{8}$$

The shear rate and the viscosity can be found provided the functional form of the viscosity is given and both the temperature and the pressure fields are known.

For later convenience, here we define the stream function as follows:

$$u = -\frac{\partial \Psi}{\partial y} G(t)\,\Phi \tag{9}$$

$$v = \frac{\partial \Psi}{\partial x} G(t)\,\Phi \tag{10}$$

Because we ignore secondary flow, the stream function depend on x, y and time only. The function $G(t)$ is related to the front location and a given pressure variation near the gate. It should be pointed out that the above two forms satisfy the continuity equation to a second order as a result of the condition that the function Φ varies weakly in x and y directions.

By substituting the above equations into Equations (5) and (6) and then cross differentiating, we obtain an equation for the pressure:

$$\frac{\partial^2 P}{\partial x^2} + \frac{\partial^2 P}{\partial y^2} = 0(\sigma^2) \tag{11}$$

Further manipulation leads to an equation for the stream function:

$$\frac{\partial^2 \Psi}{\partial x^2} + \frac{\partial^2 \Psi}{\partial y^2} = 0(\sigma^2) \tag{12}$$

It is shown that, ignoring the second order, both the stream function and the pressure for the type of non-Newtonian fluid described by Equation (1) obey the Laplace equation.

In the steps to obtain the above equations, the following conditions have been assumed:

$$\frac{1}{\Phi}\frac{\partial \Phi}{\partial x} \sim 0(\sigma^2) \tag{13a}$$

$$\frac{1}{\Phi}\frac{\partial \Phi}{\partial y} \sim 0(\sigma^2) \tag{13b}$$

Physically, the above conditions mean that the analysis is applicable to small changes in flow area and moderate variation of temperature in flow directions.

With the constraints mentioned above, we extend the theory of Hele-Shaw (Schlichting, 1968) on steady Newtonian viscous flow in narrow parallel plates to unsteady nonisothermal and non-Newtonian flows. Moreover, on the basis of the potential theory, constant streamlines and isopressure lines are orthogonal. As the surface of the progressing front is that of constant (atmospheric) pressure, therefore the profile of the melt front is also orthogonal to the streamlines. In this respect, the thin cavity approach also simplifies the determination of free surfaces, implying that the combined effects of surface tension, normal stresses, and zero shear condition (Kuo and Tanner, 1974) are negligible. In terms of the theory, the flow pattern of filling thin cavities can be mathematically described by harmonic functions or determined by a conformal mapping technique. Some analytical methods were described by Richardson (1972) on unbounded injection flows. As a matter of fact, one can easily plot flow patterns with orthogonal meshes and regard contours of cavity side walls and inserts as boundary streamlines.

Moreover, the derived Laplace equations for the pressure and the stream functions can be extended to two-dimensional injection flows bounded by curved walls with small variations in thickness and curvature. In this case x, y, and z should be a properly chosen curvilinear orthogonal system of coordinates and the local half thickness may be used to replace the integration limit a in Equation (7).

Rectangular Cavities

A study of filling rectangular cavities is of great interest, since the flow field involves the transition of a divergent radial flow to a convergent one confined by the parallel side walls after the injection front hits the cavity corners.

With reference to the Cartesian coordinate system shown in Figure 1 with its origin at the center of the gate-cavity junction and x, y, plane parallel to the cavity plates, the boundary conditions for the stream function ψ are

$$\frac{\partial \Psi}{\partial x} = 0 \qquad x > 0, y = \pm b \tag{14}$$

$$\frac{\partial \Psi}{\partial y} = 0 \qquad x = 0, |y| > c \tag{15a}$$

$$\frac{\partial \Psi}{\partial y} = -U_o(y, t) \qquad x = 0, |y| \leq c \tag{15b}$$

$$\Psi = \Psi_o \qquad x = 0, y > c; y = b \tag{16a}$$

$$\Psi = \Psi_o \qquad x = 0, y < -c; y = -b \tag{16b}$$

where b and c are the half widths of the cavity and the gate, respectively. The Laplace equation of Ψ should be solved in conjunction with the solution of pressure, satisfying the following boundary conditions:

$$P = 0 \qquad x = R_f, y = 0; X_f(y) \tag{17}$$

$$P = P_o(t) \qquad x = r_o, y = 0 \tag{18}$$

$$\frac{\partial P}{\partial x} = U_o(y, t)G(t) \qquad x = 0, |y| \leq c \tag{19}$$

Here we denote the front profile by $X_f(y)$. Note that Ψ_o is a constant, and the conditions (16a) and (16b) mean that the contours of the cavity edge are streamlines.

The forms of $U_o(y, t)$ can be determined by assuming a similarity of velocity profiles. It may be first assumed that the axial pressure gradient is uniform in the capillary gate, implying that both the function $U_o(y, t)$ and the velocity are uniform across the gate width according to Equations (15b) and (19). Based on this condition, the shear rate at the gate-cavity junction can be found through the following equation obtained by integrating Equation

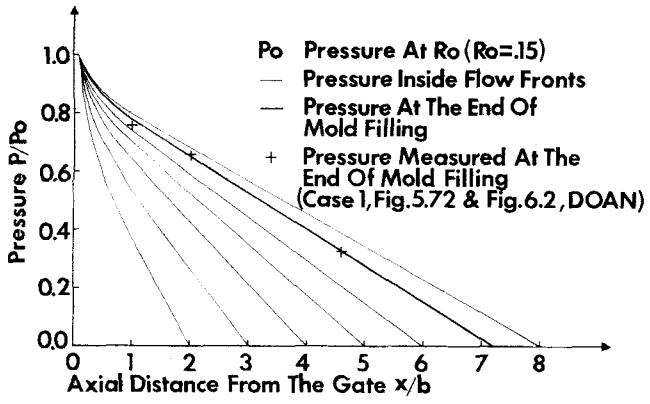

Fig. 2. Pressure drops from the gate to the flow fronts.

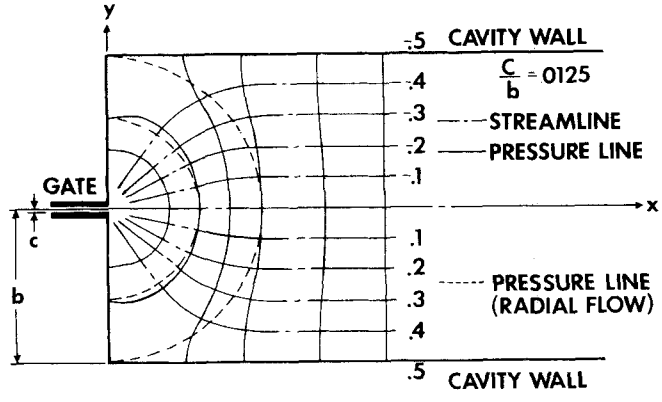

Fig. 3. The flow pattern in a cavity with a narrow gate.

(3):

$$\eta(T, \dot{\gamma}^2) \frac{\partial u}{\partial z} = \frac{\partial P}{\partial x} z \tag{20}$$

Consequently, the velocity distribution across the gap at the gate $u(o, o, z)$ can be calculated by using Equation (5). Thus, a simple means to correct the previous assumption is to assert that the form of $U_o(y)$ is similar to $u(o, o, z)$. In the boundary condition as shown in Equation (18), $P_o(t)$ is a given pressure variation in time measured at $x = r_o$, a distance away from the origin. It should be pointed out here that no-slip conditions on the cavity edges are ignored. An analysis on the boundary flow may show that a solution satisfying the preceding boundary conditions is applicable close to the side walls, up to a distance $3a$ from the wall, where a is the half thickness of the cavity.

An exact solution of the Laplace equation of Ψ satisfying the boundary conditions is

$$\Psi = \sum_{n=1}^{\infty} A_n e^{-n\pi \frac{x}{b}} \sin\left(n\pi \frac{y}{b}\right) - \frac{\Psi_o}{2} \frac{y}{b} + \frac{4E}{\pi} \sum_{n=0}^{\infty} \frac{1}{2n+1} e^{-(2n+1)\pi \frac{x}{b}} \sin\left[(2n+1)\pi \frac{y}{b}\right] \tag{21}$$

where

$$A_n = -\frac{2}{n\pi} \int_o^c U_o(y) \cos\left(n\pi \frac{y}{b}\right) dy \tag{22a}$$

$$E = \Psi_o \left(1 + \frac{c}{b}\right) - \Sigma A_n \sin\left(n\pi \frac{c}{b}\right) \tag{22b}$$

The value of Ψ and the function $U_o(y)$ are determined by the pressure and temperature distributions at the gate and the front, which are affected by a fluid's properties. To study the flow near the origin, $x = o$ and $y = o$, a power expansion technique described by Imberger (1972), for investigating two-dimensional sink flow of a stratified fluid, may be used.

In conjunction with the solution of the stream function, the pressure distributions can be found through their correlations with the velocity components. Let $R_f(t)$ denote the axial location (at $y = o$ plane) of the front at zero pressure. Then the solution of pressure is

$$\frac{P(x, y, t)}{P_o(t)} = 1 - \frac{H(x, y, t)}{H(R_f, o, t)} \tag{23}$$

where

$$H(x, y, t) = \sum_{n=1}^{\infty} A_n \left[e^{-n\pi \frac{x}{b}} \cos\left(n\pi \frac{y}{b}\right) - e^{-n\pi \frac{r_o}{b}}\right] + \frac{\Psi_o}{2}\left(\frac{x}{b} - \frac{r_o}{b}\right) + \frac{4E}{\pi} \sum_{n=0}^{\infty} \frac{1}{2n+1} \left[e^{-(2n+1)\pi \frac{x}{b}} \cos\left[(2n+1)\pi \frac{y}{b}\right] - e^{-(2n+1)\pi \frac{r_o}{b}}\right] \tag{24}$$

The above analytical expression for pressure is very useful, as it demonstrates explicitly the roles of the front location, of the pressure, and of the velocity profile at the gate (or the flow rate) in shaping the overall pressure distributions in the cavity. It will be shown later that the progression of the front, represented by $R_f(t)$, can be computed readily with the use of Equation (23). Figure 2 shows typical nondimensional pressure profiles, along the x axis, associated with different front locations. It is worth noting that the pressure profiles are not sensitive to the functional form of $U_o(y)$, which is similar to the velocity profile at the gate.

As mentioned earlier, the injection mold filling is characterized by the progression of the free (or front) surface. In fact, the determination of front shapes can be a sensitive criterion for a satisfactory numerical simulation of injection filling. In the framework of the present analysis, the computation is rather straightforward. Let $\chi(y)$ denote the x coordinate of a constant pressure line. Then, on such line a functional differentiation leads to the following equation for $\chi(y)$ as

$$\frac{d\chi}{dy} = -\frac{\partial P}{\partial y} \Big/ \frac{\partial P}{\partial x} \tag{25}$$

The pressure gradients can be readily evaluated from Equation (23). This formulation eliminates the effects of surface tension and normal stresses. To find the front shape at a specified location R_f, the computation of the above equation may start with the right-hand side evaluated at $\chi = R_f$ and $y = o$. Figure 3 shows computational front shapes and isopressure lines. The profiles vary with the effective width of the gate but are not sensitive to the velocity distribution at the gate. Also shown in the same figure are the corresponding normalized streamlines. The flow patterns agree satisfactorily with experimental observations with high-speed photography (Doan, 1974). Note that the isopressure lines shown in the figure within the radius equal to the width of the cavity are valid only after the front reaches the side walls.

Radial Flow

A radial flow prevails before the flow front confronts the parallel edges. The streamlines are straight and radial from the gate, and the front shapes are semicircular. Since the wall effects are incorporated into the boundary conditions of the foregoing solutions, the latter are not applicable to the preceding radial flow. Although this flow has been investigated elsewhere, for completeness, an analysis for such flow is outlined here.

Despite the fact that the Laplace equation can be transformed into a cylindrical coordinate to solve for the pressure field, it is more accurate to work directly on momentum equations in such a coordinate system in consideration of the diverging nature of the flow. As required by the continuity of the flow, the radial velocity V_r is inversely proportional to the radius from the gate

$$V_r = \frac{f(z,t)}{r} \tag{26}$$

In relating to the viscosity and a radial pressure gradient, the velocity can also be expressed as

$$V_r = \frac{\partial P}{\partial r}\int_a^z \frac{z'}{\eta(r,z',t)}\,dz' \tag{27}$$

which is similar in form for the two velocity components given in Equations (5) and (6). The local shear rate can be evaluated through the momentum equation if the viscosity function and the pressure gradient are known

$$\eta(T,\dot\gamma^2)\frac{\partial V_r}{\partial z} = \frac{\partial P}{\partial r}z \tag{28}$$

Unlike the previous analysis for the flow in the rectangular region, we will specify here a viscosity function to solve for the pressure profile. This approach may lead to a solution more sensitive to the change of viscosity curves. The following analysis will be based on a power law model with temperature variations. The model is

$$\eta = \eta_T|\dot\gamma|^{-n} \tag{29}$$

The parameter n is the power index associated with the slope of the viscosity curve vs. the shear rate plotted on a log-log scale. η_T denotes variation with the temperature or activation energy.

Assuming that η_T varies weakly with r, we obtain a solution for the pressure as

$$\frac{P(r,t)}{P_o(t)} = \frac{R_f^n(t) - r^n}{R_f^n(t) - r_o^n} \tag{30}$$

where $R_f(t)$ is the front location, and $P_o(t)$ denotes the pressure variation in time measured at r_o close to the gate.

Front Progression Speed

There are two independent methods for evaluating the flow rate provided the front position is known: by integrating the velocity profile over the cross-section area, and by the rate of increase of the occupied volume. As both answers are to be consistent, this requirement provides a means for finding the front's location or progression speed.

If we regard the front speed as an average velocity across the cavity gap, then the front progression along the x axis can be obtained from Equation (5) as

$$\frac{dR_f}{dt} = \frac{\partial P}{\partial x}\frac{1}{a}\int_o^a \Phi\,dz \tag{31}$$

The right-hand side should be evaluated at $x = R_f$ and $y = o$. In terms of the front speed, the flow rate Q can be expressed as

$$Q = \frac{d(\text{volume})}{dt} = 2a\frac{dA}{dR_f}\frac{dR_f}{dt} \tag{32}$$

where A is the area wetted or covered by the melt flow and is a function of the front location $R_f(t)$. Note that dA/dR_f can be evaluated through the front shape determined by Equation (25) or by an approximate profile. If the flow rate is given, then it suggests an alternative method of finding the progression speed, that is, from Equation (32):

$$\frac{dR_f}{dt} = \frac{Q}{2a\dfrac{dA}{dR_f}} \tag{33}$$

Temperature Field

Heat conduction and viscous heating contribute to temperature variations in the flow medium. They are governed by the energy equation, and its solution is to be solved simultaneously with the momentum equations.

For narrow passages, the heat transfer is considered mainly in the z or thickness direction. Manipulation of the energy equation with the thin cavity approximation leads to the following working equation of nondimensional form

$$\frac{\partial T}{\partial t} = \beta\frac{\partial^2 T}{\partial z^2} + \Gamma|zF\dot\gamma| + 0(\sigma^2) \tag{34}$$

where

$$F = \sqrt{\left(\frac{\partial P}{\partial x}\right)^2 + \left(\frac{\partial P}{\partial y}\right)^2} \qquad \frac{R_f}{b} > 1 \tag{35a}$$

$$F = \frac{\partial P}{\partial r} \qquad \frac{R_f}{b} \leq 1 \tag{35b}$$

The nondimensional quantities are defined below

$$x^* = \frac{x}{b},\ y^* = \frac{y}{b},\ z^* = \frac{z}{a},\ r^* = \frac{r}{b} \tag{36a}$$

$$T^* = \frac{T - T_w}{T_c - T_w},\ \dot\gamma^* = \frac{a\dot\gamma}{U} \qquad P^* = \frac{P}{\left(\dfrac{\eta_o U b}{a^2}\right)} \tag{36b}$$

$$t^* = \frac{ut}{b},\ \beta = \frac{bk}{a^2\rho C_p U},\ \Gamma = \frac{\eta_o b U}{\rho C_p a^2(T_c - T_w)} \tag{36c}$$

For neatness, the asterisks are dropped from the nondimensional quantities in Equation (34) and the expressions to follow.

The initial and boundary conditions of the temperature field are complicated by the mold heating and nonuniformity of melt temperature at the cavity inlet as a result of flow through the runner and the gate. Practically, they can be simplified, however, because of a fluid element's short residence time in the runner and gate, and little temperature rise in the mold.

Letting the temperature field at R_o, near the gate, be T_o, we may set the initial and the boundary conditions as

$$T_o = 1 \quad r = R_o,\ -1 < z < 1,\ t_o = 0 \tag{37a}$$

$$T_o = 0 \quad r = R_o,\ z = \pm 1,\ t_o > 0 \tag{37b}$$

where $R_o = r_o/b$. It is noted here that R_o is also the starting location in the temperature field consistent with the flow field. t_o is the time counted from the moment of the front reaching R_o. Let the temperature and the residence time of a flow element, say i, occupying a local cavity gap be T_i and t_i, respectively. Then its initial and boundary conditions are

$$T_i(R_i, z, t_i) = T_o(r_o, z, t)\ R_i = R_o,\ -1 < z < 1,\ t_i = 0 \tag{38a}$$

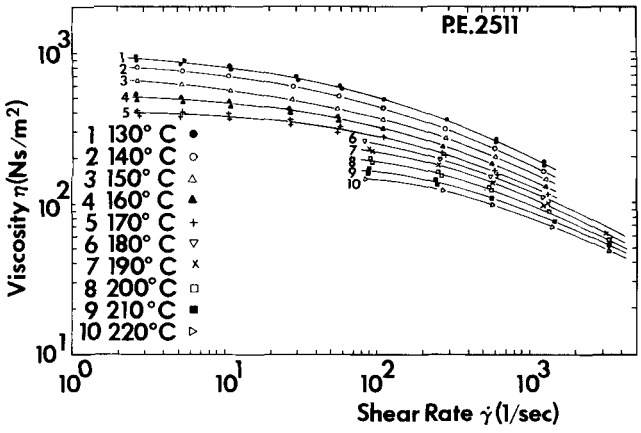

Fig. 4. Viscosity as function of shear rate and temperature, polyethylene.

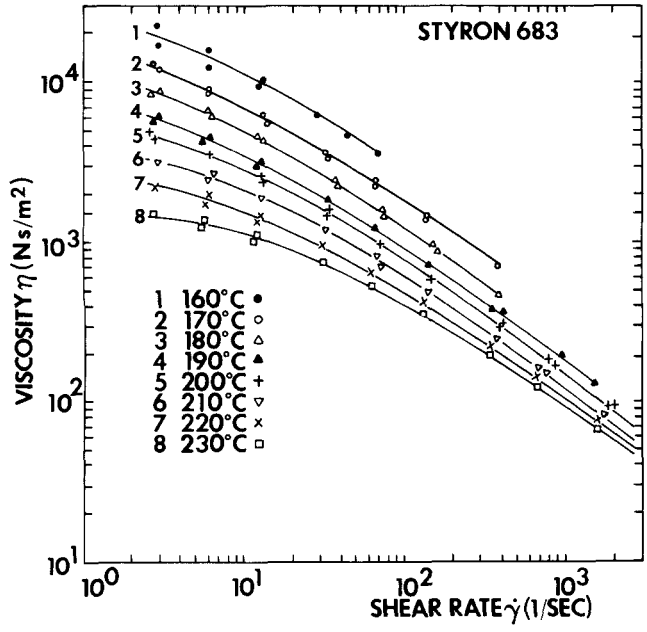

Fig. 5. Viscosity as function of shear rate and temperature, polystyrene.

$$T_i(R_i, z, t_i) = 0 \quad R_i = R_i(t_i),\ z = \pm 1,\ t_i > 0 \quad (38b)$$

Note that the mold temperature is assumed uniform as shown above. The identity of the front element is $R_i = R_f$ and $t_i = t$. In this paper all the thermal properties will be regarded as constants in the present analysis. The crystallinity and the latent heat will also be ignored.

The energy equation of heat conduction and generation have been solved by Peterson (1941) in cases of infinite and semi-infinite solids. Applying his method to the slab, we obtain the solution to Equation (34) satisfying the described conditions as

$$T(x, y, z, t) = \sum_{n=0}^{\infty} \left[A_n' \, e^{-\left(\frac{2n+1}{2}\pi\right)^2 \beta t} + \Gamma E_n \right] \cos\left(\frac{2n+1}{2}\pi z\right) \quad (39)$$

where

$$E_n = \int_o^t |F| \, e^{\left(\frac{2n+1}{2}\pi\right)^2 \beta(\lambda - t)} \, d\lambda \int_o^1 2|\dot{\gamma}|z \cos\left(\frac{2n+1}{2}\pi z\right) dz \quad (40)$$

The proper forms of the function F are given in Equations (35a) and (35b). Instead of integrating from o to t, we can rewrite the right-hand side of Equation (40) in a form so that E_n can be evaluated in terms of its preceding value and current values of F and $\dot{\gamma}$. By relating the coordinates, the residence time, and the flow quantities to a flow element followed, the above solution gives the temperature history of that element. In that case, A'_n is the Fourier component of the initial temperature of that element given in Equation (38a). For the element and the temperature field at R_o, A'_n is $(4/\pi)(-1)^n/(2n + 1)$.

COMPUTATIONS AND RESULTS

In the foregoing analysis, the equations and solutions are written in three-dimensional forms. For rigorous computations, one can establish a system of equations to solve for the front speed and the temperature and other flow quantities at any point inside the cavity. Nevertheless, one of the advantages of the present method is that one only needs to calculate the temperature and the flow quantities on the symmetric plane ($y = o$). From the values computed in this plane, isolines of such quantities can be extended to any other points of interest in the cavity. Usually the determination of the isolines by using the pressure or the stream function is a much easier task.

To start computation, an initial value of pressure gradient is needed. Assuming that the temperature is rather uniform when the front enters the cavity, we estimate the value of nondimensional pressure gradient at R_o to be

$$\frac{\partial P^*}{\partial r^*} = -\left(\frac{dP^*}{dt^*}\,\frac{3-2n}{1-n}\right)^{\frac{1-n}{2-n}} \quad r^* = \frac{r_o}{b},\ t^* = 0 \quad (41)$$

It is obtained through the use of a pressure profile of the radial flow given in Equation (30) and a velocity solution. The rate of pressure increase is known from a given pressure input $P_o(t)$ at R_o. At this location, which is close to the gate, the heat transfer is two dimensional, similar to the cooling of the gate. To account for this additional cooling and for the sake of convenience, we assume that the magnitude of the second derivative of temperature in y is close to that in z because the dimensions of the gate width and the thickness are close. With this approximation, we simply replace β by 2β in Equation (34) to calculate the heat transfer at R_o. This correction is significant since the data at R_o, or at the gate, are related to the whole flow field.

Then the subsequent computations are as follows. After Equation (41) is used, the shear rate distribution may be calculated so that the temperature profile can be determined. These two data shall be used for finding the viscosity variations. Based on the latter values, we can compute velocity distributions, the flow rate, and the front speed. Consequently, a new front position is located, and a new pressure gradient is evaluated with reference to a given pressure increase over a small time increment. These steps are repeated in time by using radial flow equations until the front reaches the cavity edges, since then all the flow quantities are governed by the pressure and the stream function imposed in the rectangular domain.

For comparison with laboratory results, our computations are based on the experimental data given by Doan

TABLE 1. RESIN CHARACTERISTICS

Main characteristics	DuPont P.E. 2511 low density	DuPont P.E. 2907 high density	Dow Chemical P.S. styron 683
Thermal properties			
Density (g/cm³)	0.940	0.960	0.978
Specific heat (kJ/kg K)	2.53	2.57	2.34
Thermal conductivity (W/m K)	0.199	0.216	0.0976
Rheological characteristics			
n	0.296	0.345	0.632
$\Delta E/R$ (1/°K)	2 115	1 580	5 910
Ac (mNs · s^{-n}/m^2)	0.938×10^5	1.63×10^6	0.885×10^4
Lower bound (s^{-1})	10	10	10
Upper bound (s^{-1})	10^4	10^4	10^4

(Assuming $\eta = Ac \exp(\Delta E/RT)\,|\dot{\gamma}|^{-n}$, T in K and $\dot{\gamma}$ in s^{-1})

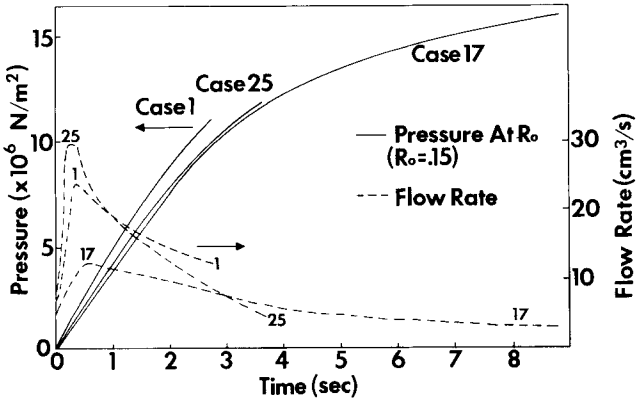

Fig. 6. Pressure measured near a gate and calculated flow rates.

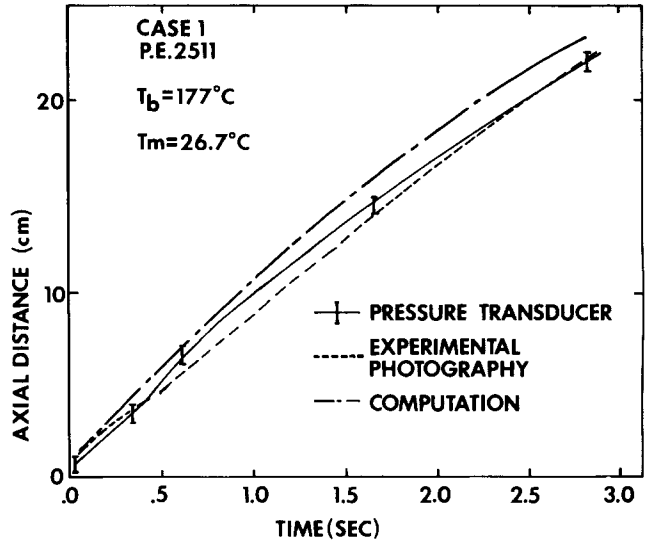

Fig. 7. Progression of flow front, P.E. 2511.

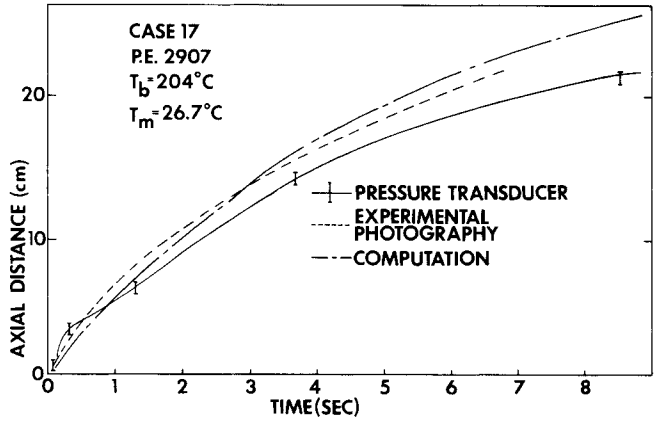

Fig. 8. Progression of flow front, P.E. 2907.

(1974). The experiments were carried out in a Metalmec 2-1/3 oz reciprocating screw injection molding machine, and the materials were commercial polyethylene and polystyrene resins. These two resins represent different rheological behaviors. Polystyrene is amorphous and more susceptible to changes in temperature and shear rate, while polyethylene is less sensitive but will be crystallized upon cooling. For illustration, the viscosity variations of these two resins are shown in Figure 4 and Figure 5. Their thermal and rheological characteristics are given in Table 1. The trends of the data are approximated by using power law models with upper and lower bounds. The dependency on temperature is described by an exponential function of reciprocal temperature. We select typical cavity pressures, measured at 0.476 cm from the gate, representing two resins and wide variations of molding conditions as our pressure inputs $P_o(t)$ for computations. They are shown as case 1, case 17, and case 25 in Figure 7, in which R_o denotes a nondimensional distance from the gate. All of these data were obtained with a rectangular cavity with the dimensions of 0.318 cm × 6.35 cm × 22.9 cm. It should be mentioned here that in these experiments the cavity walls ($z = \pm a$) were cooled by air maintained at 26.7°C. No appreciable temperature gradients were imposed in width and length directions.

With given pressure inputs, the computed flow rates are also shown in Figure 6. It is certainly feasible that one can establish a computing scheme in which the flow rate is taken as a given boundary condition. In that case, the cavity pressure can be predicted. The illustrated results show that the flows are accelerated in the early phase of injection in these particular experimental runs. The accuracies of both computational and experimental results are represented in Figures 7, 8, and 9. Note that the molding conditions involve low and high temperatures with slow and fast injection speeds. Because of the sizes of the pressure transducers and the meniscuses of the front between two narrow plates, there are discrepancies between the readings of the transducer and the high-speed pho-

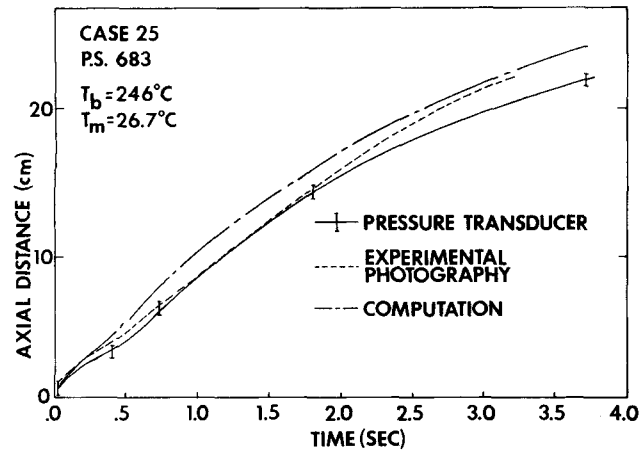

Fig. 9. Progression of flow front, P.S. 683.

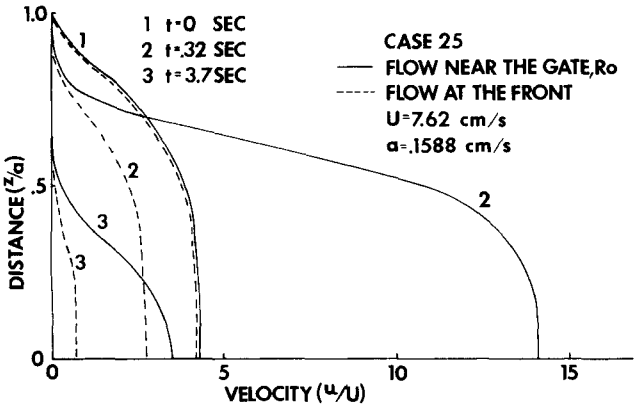

Fig. 11. Velocity distributions in the cavity gap.

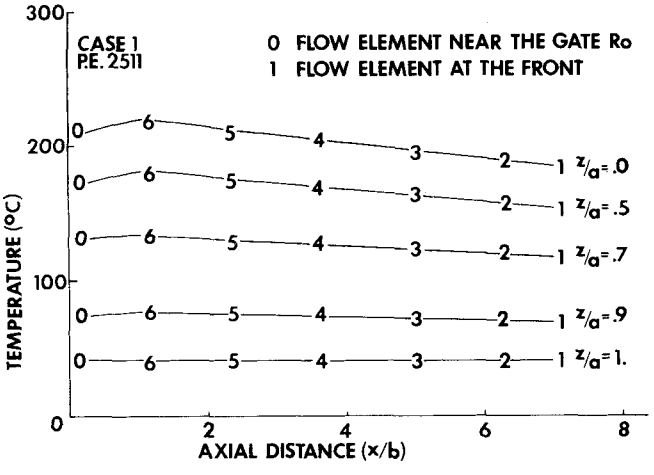

Fig. 12. Temperature distributions from the gate to the cavity end.

tography in tracing the front advancement. In comparing the front locations at a given time with these cases and other experimental results reported (Doan, 1974), most of our computational results show less than 15% error. The accuracy can also be tested by comparing the pressure drops from the gate to the front such as the one already shown in Figure 2.

Owing to viscous heating and cooling of the mold, the resultant temperature field is complex. Figure 10 shows typical temperature profiles across the cavity gap near the gate and at the front at different times. There are substantial effects of temperature on the velocity profiles as evidenced in Figure 11. It shows immobility of growing frozen layers close to the cold walls. Furthermore, one can visualize that the flowable central portion of the cavity

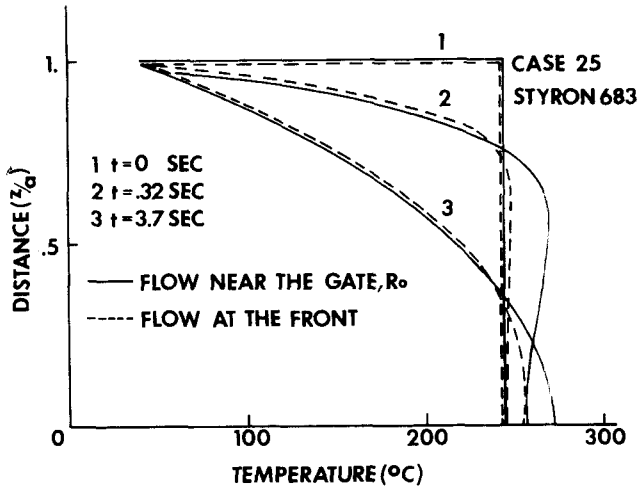

Fig. 10. Temperature distributions in the cavity gap.

is the channel for melt transportation to form a new advancing front.

Figure 12 shows the temperature distribution across the cavity at the end of filling. The computational result is accomplished by following well-spaced fluid elements entering the cavity. In view of the fact that the fluid elements lined up across the gap at a location x and y are not the same elements entering the cavity, the method employed yields only approximate results. It is interesting to note that the figure shows little temperature variation in the flow direction. This is partly due to the fact that the temperature distribution in the gate is that of the outgoing fluid element. Moreover, the result justified our previous assumption of small temperature gradients in the flow directions.

In summary, it is shown that the use of a generalized viscous model can closely simulate the behaviors of thermoplastics in injection filling thin cavities. Besides, the flow patterns can be described by the Laplace equations in the case of small variation in flow area and moderate change of temperature in main flow directions.

ACKNOWLEDGMENT

The authors wish to express their thanks to the National Research Council, Ministry of Education of Province of Quebec, McGill University, Minnesota Mining and Manufacturing Company, and the Electrical Components Division of Bendix Corporation for their supports in this work.

NOTATION

a, b = half thickness and half width of a rectangular cavity, respectively
c = half width of a gate
C_p = specific heat
$G(t)$ = time function defined in Equations (9) and (10)
k = thermal conductivity
P = pressure
$P_o(t)$ = given pressure profile at r_o
r = radial coordinate with origin at gate-cavity junction
R_f = location of progressing front along x axis
r_o = location of pressure transducer near the gate
R_o = nondimensional distance, r_o/b
t = time
T = temperature
U = reference velocity
U_o = axial velocity component at the cavity entrance
V_r = radial velocity
X_f = profile of flow front
x, y, z = Cartesian coordinate system, see Figure 1

Greek Letters

$\dot{\gamma}$ = shear rate
η = shear viscosity
η_o = reference viscosity
η_T = temperature function defined in Equation (29)
ρ = density
τ = shear stress
Φ = derived function as defined in Equation (7)
χ = x coordinate of a isopressure line
Ψ = stream function
Ψ_o = constant, see Equations (16a) and (16b)
T_w = mold wall temperature
T_c = melt temperature (or barrel temperature)

LITERATURE CITED

Doan, P. H., "Injection Molding of Thermoplastics in Rectangular Cavities," M. Eng. Thesis, McGill University, Canada (1974).

Imberger, J., "Two-Dimensional Sink Flow of a Stratified Fluid Contained in a Duct," *J. Fluid Mech.*, **53**, 329 (1972).

Kamal, M. R., and S. Kenig, "Injection Molding of Thermoplastics," *Polymer Eng. Sci.*, **12**, 294 (1972).

Kamal, M. R., Y. Kuo, and P. H. Doan, "The Injection Molding Behavior of Thermoplastics in Thin Rectangular Cavities," *ibid.*, **15**, 863 (1975).

Kuo, Y., Ph.D. thesis, "The Determination of the Second Normal Stress Difference in Viscoelastic Flows," Brown Univ., Providence, R. I. (1973).

———, and R. I. Tanner, "On the Use of Open-Channel Flows to Measure the Second Normal Stress Difference," *Rheol. Acta*, **13**, 443 (1974).

Laurencena, B. R., and M. C. Williams, "Radial Flow Between Parallel Plates," *Trans, Soc. Rheol.*, **18**, 331 (1974).

Lord, H. A., and G. Williams, "Mold-Filling Studies for the Injection Molding of Thermoplastic Materials. Part II: The Transient Flow of Plastic Materials in the Cavities of Injection-Molding Dies," *Polymer Eng. Sci.*, **15**, 569 (1975).

Menges, G., and G. Wubken, "Influence of Processing Conditions on Molecular Orientation in Injection Molding," *SPE Tech. Papers, 19, 519,* 31st ANTEC (1973).

Paterson, S., "The Conduction of Heat in a Medium Generating Heat," *Phil. Mag.*, **32**, No. 7, 384 (1941).

Richardson, S., "Hele Shaw Flows with a Free Boundary Produced by the Injection of Fluid into a Narrow Channel," *J. Fluid Mech.*, **56**, 609 (1972).

Schlichting, H., *Boundary Layer Theory*, 2 ed., p. 114, McGraw-Hill, New York (1968).

Schmidt, L. R., "A Special Mold and Tracer Technique for Studying Shear and Extensional Flows in a Mold Cavity During Injection Molding," *Polymer Eng. Sci.*, **14**, 797 (1974).

Tanner, R. I., "Plane Creeping Flows of Incompressible Second-Order Fluids," *Phys. Fluids*, **9**, 1246 (1966).

White, J. L., "Fluid Mechanical Analysis of Injection Mold Filling," *Polymer Eng. Sci.*, **15**, 44 (1975).

———, and H. B. Dee, "Flow Visualization for Injection Molding of Polyethylene and Polystyrene Melts," *ibid.*, **14**, 212 (1974).

Wu, P.-C, C. F. Huang, and C. G. Gogos, "Simulation of the Mold-Filling Process," *ibid.*, 223 (1974).

Manuscript received December 23, 1975; revision received March 23, and accepted March 24, 1976.

Turbulent Drag Reduction in Dilute Fiber Suspensions: Mechanistic Considerations

Both fibrous and polymeric additives, used alone or in combination, appear to affect primarily the fluid in the sublayer region adjacent to a solid surface, contrary to previous predictions. An analysis of fluid deformation modes shows tentatively why drag reduction levels become less sensitive to system scale when fibrous additives are employed, and why polymeric and fibrous additives may be more effective in combination than when either additive is used alone.

D. D. KALE

and

A. B. METZNER

Department of Chemical Engineering
University of Delaware
Newark, Delaware 19711

SCOPE

Drag reduction, under turbulent flow conditions, has been observed in solutions of synthetic as well as natural polymers, in suspensions of solid particles, and in micellar systems. Comprehensive and readable accounts have been provided in recent years by Savins (1967, 1969), Kenis (1968), Hoyt (1972*a*, 1972*b*), Little et al. (1975), and Virk (1975). Mechanistic interpretations of the phenomenon in polymer solutions have centered on the viscoelastic (nonlinear) fluid properties for many years (Dodge and Metzner, 1959; Metzner and Park, 1964; Astarita, 1965; Gadd, 1965). Seyer and Metzner (1966, 1969) introduced arguments concerning the high resistance of viscoelastic media to elongational deformations, and Hansen (1973) and Ruckenstein (1971) focused upon the low resistance to deformation of viscoelastic media when deformed on time scales which are small in comparison to the natural time of the medium.

Suspensions of solid particles, especially fibrous ones, exhibit a number of pragmatic advantages over polymers when use of additives is considered for drag reduction purposes: they offer a much greater resistance to degradation, their efficacy is less sensitive to the scale of the process, and they may be removed from the fluid more

Correspondence concerning this paper should be addressed to A. B. Metzner. D. D. Kale is now with the University of Bombay, Matunga, Bombay 19.